NanoImpact 29 (2023) 100444

Contents lists available at ScienceDirect

NanoImpact

journal homepage: www.elsevier.com/locate/nanoimpact

Apoplast utilisation of nanohaematite initiates parallel suppression of *RIBA1* and *FRO1&3* in *Cucumis sativus*

Amarjeet Singh [a,b], Maria Gracheva [c,d,e], Viktória Kovács Kis [e,f], Áron Keresztes [g], Máté Sági-Kazár [a,b], Brigitta Müller [a], Fruzsina Pankaczi [a,b], Waqas Ahmad [a,b], Krisztina Kovács [c], Zoltán May [h], Gyula Tolnai [i], Zoltán Homonnay [c], Ferenc Fodor [a], Zoltán Klencsár [e], Ádám Solti [a,*]

[a] Department of Plant Physiology and Molecular Plant Biology, Institute of Biology, ELTE Eötvös Loránd University, Pázmány Péter sétány 1/C, Budapest H-1117, Hungary
[b] PhD School of Biology, ELTE Eötvös Loránd University, Pázmány Péter sétány 1/A, Budapest H-1117, Hungary
[c] Laboratory of Nuclear Chemistry, Institute of Chemistry, ELTE Eötvös Loránd University, Pázmány Péter sétány 1/A, Budapest H-1117, Hungary
[d] Hevesy György PhD School of Chemistry, ELTE Eötvös Loránd University, Pázmány Péter sétány 1/A, Budapest H-1117, Hungary
[e] Centre for Energy Research, Eötvös Loránd Research Network, Konkoly-Thege Miklós út. 29-33, Budapest H-1121, Hungary
[f] Institute of Environmental Sciences, University of Pannonia, Egyetem út. 10, Veszprém H-8200, Hungary
[g] Department of Plant Anatomy, Institute of Biology, ELTE Eötvös Loránd University, Pázmány Péter sétány 1/C, Budapest H-1117, Hungary
[h] Research Centre for Natural Sciences, Eötvös Loránd Research Network, Magyar tudósok körútja 2, Budapest H-1117, Hungary
[i] Kondorosi út 8/A, 1116 Budapest, Hungary

ARTICLE INFO

Editor: Dr. Phil Demokritou

Keywords:
Energy dispersive spectroscopy elemental mapping
Cucumber
Ferric reductase Oxidase
High-resolution transmission electron microscopy
Mössbauer spectroscopy
Riboflavin

ABSTRACT

Nanoscale Fe containing particles can penetrate the root apoplast. Nevertheless, cell wall size exclusion questions that for Fe mobilisation, a close contact between the membrane integrating FERRIC REDUCTASE OXIDASE (FRO) enzymes and Fe containing particles is required. Haematite nanoparticle suspension, size of 10–20 nm, characterized by ^{57}Fe Mössbauer spectroscopy, TEM, ICP and SAED was subjected to Fe utilisation by the flavin secreting model plant cucumber (*Cucumis sativus*). Alterations in the structure and distribution of the particles were revealed by ^{57}Fe Mössbauer spectroscopy, HRTEM and EDS element mapping. Biological utilisation of Fe resulted in a suppression of Fe deficiency responses (expression of *CsFRO 1, 2 & 3* and *RIBOFLAVIN A1*; *CsRIBA1* genes and root ferric chelate reductase activity). Haematite nanoparticles were stacked in the middle lamella of the apoplast. Fe mobilisation is evidenced by the reduction in the particle size. Fe release from nanoparticles does not require a contact with the plasma membrane. Parallel suppression in the *CsFRO 1&3* and *CsRIBA1* transcript amounts support that flavin biosynthesis is an inclusive Fe deficiency response involved in the reduction-based Fe utilisation of *Cucumis sativus* roots. CsFRO2 is suggested to play a role in the intracellular Fe homeostasis.

1. Introduction

Iron (Fe) is an essential element for living organisms. In the environment, it is available in a wide variety of primary and secondary soil minerals (Mimmo et al., 2014). Poorly soluble Fe(III) oxides such as haematite (α-Fe_2O_3) commonly occur in soil (Colombo et al., 2014; Krämer et al., 2006; Mimmo et al., 2014). Agricultural soils mainly comprise of oxic environments where Fe is found in insoluble precipitates (Lemanceau et al., 2009). Thermodynamically, haematite is the most stable form of the ferric (hydro-) oxides and the least soluble as well (Jang et al., 2007; Marshall et al., 2014). Haematite nanoparticles (NH) can also be formed under environmental conditions in the soil. With their high surface area Fe containing nanoparticles represent a good source of Fe that can be utilised by Strategy I plants. Release of Fe from Fe oxide nanoparticles enables the regeneration of plant Fe deficiency. (Zhu et al., 2008; Rui et al., 2016; Shimizu et al., 2016). Although ferric oxides are important sources of the bioavailable fraction of Fe for plants, little is known about the ways of utilisation. Although

Abbreviations: dFe, iron deficient; FCR, Ferric Chelate Reductase; NH, nanohaematite; oFe, plants grown on iron.

* Corresponding author.
E-mail address: adam.solti@ttk.elte.hu (Á. Solti).

https://doi.org/10.1016/j.impact.2022.100444
Received 30 August 2022; Received in revised form 13 November 2022; Accepted 27 November 2022
Available online 5 December 2022

nanoparticles are generally kept small enough to penetrate the roots, less attention is paid on the size exclusion filter property of the cells walls of plants that might limit particles to get into contact with the plasma membrane.

To cope with low bioavailability of Fe, the majority of higher plants operates the reduction-based Strategy I which strategy involves the reduction of Fe from Fe(III) to Fe(II) mediated by root plasma membrane localized FERRIC REDUCTASE OXIDASE (FRO) family proteins. In *Arabidopsis*, FRO2 is responsible for the root ferric chelate reductase activity, whereas FRO family protein members but Fe deficiency responses, too, are proposed to be more diverse and complex in other dicots. In cucumber (*Cucumis sativus*) roots, the expression of three *FRO* family genes: *CsFRO1*, *CsFRO2* and *CsFRO3*, sensitive to Fe nutrition, was linked to ferric chelate reductase activity (Waters et al., 2014; Marastoni et al., 2019). FROs are transmembrane enzymes with a ferric reductase domain on the external side (Schagerlöf et al., 2006). In *Arabidopsis*, liberated Fe(II) is transported across the plasma membrane by IRON REGULATED TRANSPORTER 1 (IRT1). *FRO2* and *IRT1* are co-regulated and dependent upon the action of basic helix-loop-helix (bHLH) FER-like Iron deficiency-induced Transcription factor (FIT). FIT forms heterodimers with one of the four bHLH proteins from subgroup Ib (bHLH38, bHLH39, bHLH100 and bHLH101) to activate downstream Fe deficiency targets (for review, see: Schwarz and Bauer, 2020; Gao and Dubos, 2021; Riaz and Guerinot, 2021). Suppression of the Fe deficiency responses relies on the sensing of Fe by hemerythrin domain Brutus (BTS), BTS-like 1&2 E3 ubiquitin ligases that target IVc family bHLHs, upstream regulators of Fe signalling, resulting their degradation (Rodríguez-Celma et al., 2019; Gao and Dubos, 2021). P-type plasma membrane H^+-ATPases contribute to the operation of Strategy I by enhancing Fe(III) solubility by decreasing rhizosphere/apoplast pH (Santi and Schmidt, 2009; Pavlović et al., 2013). Certain Strategy I plants such as *Medicago truncatula*, *Beta vulgaris* and cucumber secrete flavin derivatives under Fe deprivation. These flavin derivatives were suggested to take part in the mobilisation of Fe for the uptake (Shinmachi et al., 1997; Rodríguez-Celma et al., 2011; Pavlović et al., 2013; Sisó-Terraza et al., 2016; Satoh et al., 2016) but also to increase the availability of Fe by ferric Fe reduction and/or chelation in soil (Sisó-Terraza et al., 2016). Moreover, flavin derivatives were also shown to be able to catalyze NADH/NAD and Fe(III)/Fe(II) redox reactions (Koochana et al., 2021). The expression of genes involved in riboflavin biosynthesis is triggered under Fe deficiency (Rellán-Álvarez et al., 2010; Hsieh and Waters, 2016). Rodríguez-Celma et al. (2013). Nevertheless, indirect effect of flavin derivatives by modifying the microbial population in rhizosphere was also showed that could also impact the bioavailability of Fe in the soil (Gheshlaghi et al., 2021). Thus, the impact of flavin secretion on the reduction-based Fe uptake strategy is still debated.

Although acidification of the rhizosphere is a common Fe deficiency response among Strategy I plants, NH particles are resistant to low pH range. NH exposition restore the Fe deficiency of Strategy II plants, the utilisation of ferric oxide nanoparticles, indeed, has not been clarified properly. Thus, here we aimed to reveal the way of NH utilisation in a flavin secreting Strategy I plant model and to reveal the inclusiveness of flavin biosynthesis in Strategy I Fe uptake.

2. Materials and methods

2.1. Preparation of the nanomaterial suspension

The NH colloid suspension sample was prepared *via* forced hydrolysis process (Matijević, 1985). To enable Mössbauer spectroscopy analysis NH colloid suspension was also prepared from $FeCl_3$ enriched in ^{57}Fe. Briefly, a solution of 0.5 M $FeCl_3 \times 6H_2O$ was prepared with a volume of 50 ml, along with a separate 30 ml solution of 1% polyethylene glycol (Priowax 200, Lamberti Chemicals, Gallarate, Italy) surfactant. The latter solution was administered to 600 ml deionized water at 80 °C, with subsequent 10 min of stirring. The $FeCl_3$ solution was then added to the obtained polyethylene glycol solution with a rate of 2 ml min^{-1}, with an additional 2 h of stirring at 80 °C. The pH of the solution was adjusted to 1.75 with the addition of 10% (V/V) HCl solution, leading to partial dissolution of the precipitates. The resulting solution was boiled for 15 min, which led to the complete dissolution of the precipitates and the formation of the acidic environment resistant colloid suspension used subsequently in the experiments. To prevent the aggregation of particles and preserve the stability of the colloid sample, as for gentle method, nanoparticle concentration of the resulting suspension was fourfold increased by evaporation under vacuum.

2.2. Physico-chemical properties of the nanomaterial suspension

Transmission electron microscopy (TEM) and selected area electron diffraction (SAED) measurements were performed using an FEI Themis G2 C_s corrected microscope (FEI, Thermo Fischer, Schottky FEG electron source) equipped with a four segment Super-X EDS detector. During the measurements 200 keV accelerating voltage was applied, which allows 0.08 nm resolution in high resolution (HR)TEM mode and 1.6 nm resolution in scanning (S)TEM mode. Measurements were recorded by a 4kx4k Ceta camera using Velox software (Themo Fischer). For TEM investigation a drop of the colloid suspension was deposited onto an ultrathin carbon coated copper TEM grid (Ted Pella). The HRTEM images were analysed using Velox (FEI) software. Particle size analysis was performed in ImageJ (https://imagej.nih.gov/ij/) version 1.53u. To test the dissolution of the nanoparticles in the colloid suspension, 500 µl NH colloid suspension was filtered using pre-rinsed 3 kDa centrifugal ultrafilter (Amicon Ultra 3 K, Merck Millipore) at 5000 ×*g*, 30 min). NH colloid suspension was also subjected to centrifugal filtering after setting the pH to 5.0. Dissolution was also analysed by high-speed centrifugation. 500 µl NH was diluted to 10 ml (20× diluted) in 500 mM MES-KOH, pH 5.0 then samples were vortexed several times during a 30-min period. The pH of the solution was checked. Colloidal suspension was pelleted at 140000 ×*g*, 10 °C, 24 h in a swing-out rotor (Sw40Ti) using a Beckman L7 ultracentrifuge. 5 ml top fraction of the supernatant was carefully removed by syringe. Fe content was analysed by ICP-OES (simultaneous Spectro Genesis ICP-OES with axial plasma viewing system; SPECTRO Analytical Instruments GmbH, Kleve, Germany).

2.3. Plant material

Strategy I plant model cucumber (*Cucumis sativus* L. cv. Joker F1) was used. Seeds were germinated on wet filter papers in dark at 26 °C for two days and treated subsequently with 0.5 mM $CaSO_4$ solution for 24 h in darkness. Seedlings were then transferred to unbuffered modified quarter-strength Hoagland solution (1.25 mM KNO_3; 1.25 mM $Ca(NO_3)_2$; 0.5 mM $MgSO_4$; 0.25 mM KH_2PO_4; 11.6 µM H_3BO_3; 4.5 µM $MnCl_2$; 0.19 µM $ZnSO_4$; 0.12 µM Na_2MoO_4; 0.08 µM $CuSO_4$. Plants of optimal Fe nutrition (oFe) received 10 µM Fe(III)-EDTA additionally. Iron deficient plants (dFe) were cultivated on an Fe-free medium. The pH of the fresh nutrient solutions was pH 4.8–5.2. Three seedlings were planted in a single pot containing 400 ml nutrient solution and solution was replaced 3 times per week. Plants were grown in growth chamber under 70% relative humidity, 120 µmol m^{-2} s^{-1} photosynthetic photon flux with light periods being set from 6:00 am to 20:00 pm (14 h).

2.4. ^{57}Fe Mössbauer spectroscopy

Three weeks dFe old cucumber plants were treated with ^{57}Fe-NH colloid suspension at 100 µM nominal Fe concentration. 30 min and one week treatment times were applied. Roots were excised, blotted with filter paper and immediately frozen and stored in liquid nitrogen until measurements, in order to prevent any appreciable subsequent chemical transformation in the samples. ^{57}Fe Mössbauer spectroscopy measurements were performed on the frozen colloid suspension and plant

samples at liquid nitrogen temperature ($T = 80$ K) as in Kovács et al. (2016), using a conventional Mössbauer spectrometer (WissEl, Starnberg, Germany) operating in the constant acceleration mode with ^{57}Co (Rh) source. The Mössbauer spectra were evaluated as in Kovács et al. (2016).

2.5. Transmission electron microscopy and energy-dispersive X-ray spectroscopy on biological samples

Three weeks old dFe cucumber plants were treated with NH colloid suspension at 20 μM nominal Fe concentration for one week, where the nutrient solution was replaced three times per week to ensure the optimum Fe supply of plants. For TEM analysis, root tips were treated as in Mihailova et al. (2020). 60 nm ultrathin sections were cut by ultramicrotomy and examined in a Hitachi 7100 electron microscope (Hitachi Ltd., Tokyo, Japan). TEM micrographs were taken with a MegaView III camera (Soft Imaging System, Münster, Germany). To investigate the identity of the Fe containing nanoparticles, high resolution (HR) TEM and energy dispersive X-ray spectroscopy (EDS) were performed using the same Themis TEM at 200 keV accelerating voltage as for the nanomaterial suspension. Before the TEM study at 200 keV, the sections of root tips were covered by *ca.* 10 nm thick amorphous carbon layer to ensure thermal and electrical conductivity and thus, stability under the electron beam. HRTEM mode of the Themis microscope was applied for the atomic resolution imaging of the nanoparticles, which, after determining zone axis orientation and characteristic interplanar spacings based on Fast Fourier Transforms (FFTs), allows identification of the crystalline phase of the Fe-oxide nanoparticle. STEM mode was applied for average atomic number (Z) contrast imaging, using the high angle annular dark field (HAADF) detector of the microscope. In these images, supposing uniform sample thickness, intensity can be directly related to average atomic number. Areas of higher average atomic number appear brighter, while areas of lower average atomic number are darker and thus biological structures are easily recognizable due to the previously performed contrasting treatment. Areas for EDS elemental mapping were selected on HAADF images. EDS mapping was performed in STEM mode by recording spectrum images (SI) from the areas of interest. Offline Fourier transformation of the atomic resolution images of the nanoparticles, pixel-by-pixel post procession of the spectrum images together with the extraction of quantitative elemental concentration data were performed using the Velox software (FEI). Particle size analysis was performed in ImageJ (https://imagej.nih.gov/ij/) version 1.53u.

2.6. Recovering iron deficiency responses

Three weeks old dFe cucumber plants were treated with NH colloid suspension at 20 μM nominal Fe concentration. Recovery treatments started precisely at 9:00 am in each repetition. As for positive and negative controls, oFe and dFe plants were used, respectively. The chlorophyll content of leaves was estimated by Chlorophyll Meter SPAD-502 device (Minolta Camera Co., Osaka, Japan). Ferric chelate reductase assays were performed as in Kovács et al. (2009). Absorbance of the [Fe(II)-bathophenanthroline disulfonate$_3$]$^{4-}$ complexes was measured at 535 nm (UV-2100, Shimadzu, Kyoto, Japan). According to Smith et al. (1952) the absorption coefficient of 22.14 mM^{-1} cm^{-1} was applied.

2.7. Bioinformatics

Cucumber coding and protein sequences were retrieved using Phytozome 13 (https://phytozome.jgi.doe.gov/pz/portal.html) and CuGenDB (http://cucurbitgenomics.org) servers. Fe deficiency sensitive *FRO* genes expressing in cucumber roots were names as in Marastoni et al. (2019), to avoid any confusion with different nomenclature by Waters et al. (2014). Protein sequence to translated nucleotide sequence blast (tblastn) was performed using NCBI Basic Local Alignment Search Tool (https://blast.ncbi.nlm.nih.gov/Blast.cgi). AtFRO2 (At1g01580); AtFRO7 (At5g49740); OsFRO1 (LOC_Os04g36720) protein sequences were accessed at Aramemnon v. 8.1 server (http://aramemnon.botanik.uni-koeln.de/). Multiple protein sequence alignment was performed using Clustal Omega v. 1.2.4 server (https://www.ebi.ac.uk/Tools/msa/clustalo/). To identify the presence of intracellular signal peptides on translated protein sequence, SignalP v.4.1 server was applied (https://services.healthtech.dtu.dk/service.php?SignalP-4.1). Prediction on the identity of the cutoff signal peptide was analysed by PProwler Subcellular Localisation Predictor v.1.2 server (http://bioinf.scmb.uq.edu.au:8080/pprowler_webapp_1-2/index.jsp).

2.8. Expression analysis

Root samples (80–120 mg fresh weight) were frozen and stored in liquid nitrogen. Messenger RNA isolation was performed using the GenoVision mRNA isolation kit (Qiagen) according to the manufacturer's instructions. After recovery, mRNA samples were separated in 25 μl diethyl pyrocarbonate-treated deionized water and RNA contents were measured by NanoDrop1000 (Thermo Fisher Scientific). Residual genomic DNA contamination was digested by RNase-free DNase I (Thermo Fisher Scientific). Reverse transcription of the RNA pool was performed using oligo-dT nucleotides by ReverAid Reverse Transcriptase (Thermo Fisher Scientific) at 42 °C for 45 min and 70 °C for 10 min. For further application, cDNA samples were stored at −80 °C. Primer sequences were designed using NCBI primer designing tool (oligonucleotide primer sequences are listed in Table S1). Relative transcript amounts were measured using StepOnePlus Real-Time PCR system (Applied Biosystems) with the StepOne™ v.2.2.3 software as in Müller et al. (2019). Relative expression analysis was done according to Pfaffl (2001).

2.9. Statistical analysis

To measure the particle size distribution in the NH colloid suspension and in the biological matrix (root tip ultrathin sections), $n = 221$ and 547 particles, respectively, were subjected to size analysis. Kolmogorov-Smirnov goodness-of-fit test was applied as normality test. Based on the result of the normality test, non-parametric Mann-Whitney test was applied using InStat v. 3.00 (GraphPad Software, Inc., San Diego, CA, USA) to compare the particle populations. Biological measurements were repeated in three (biologically) independent repetition. Each set consisted of 6 plant individual of identical developmental stage per Fe treatment and per experiment. Four parallel RNA samples (technical replicates) were isolated from each three independent experiments (biological replicates). One-way ANOVA tests with Tukey-Kramer *post-hoc* tests were performed on data using InStat v. 3.00. The term 'significantly different' means that the similarity of samples is $P < 0.01$.

3. Results

3.1. Physico-chemical properties of the suspension

TEM and SAED measurements were performed on the four-time concentrated NH suspension, revealing the sample to be composed of nanocrystalline haematite colloid particles with a particle size typically lying in the 10–20 nm range (Fig. 1). Size analysis of the particles indicated 14.16 ± 6.38 nm particles (Fig. A1A,C,E; Table A2). Dissolution of the NH suspension was tested both at native pH and at pH 5.0. Centrifugal filtering of the NH colloid suspension resulted in the transmission of 2.811 ± 0.141% of the total Fe content of the suspension into the filtered phase. At pH 5.0, the transmission was 0.012 ± 0.001% of the initial Fe content of the NH colloid suspension. Dissolution of the colloidal suspension was also tested by overnight high-speed centrifugation at pH 5.0. Centrifugation resulted in a significant pelleting, which represented most of the Fe content of the material. However, the

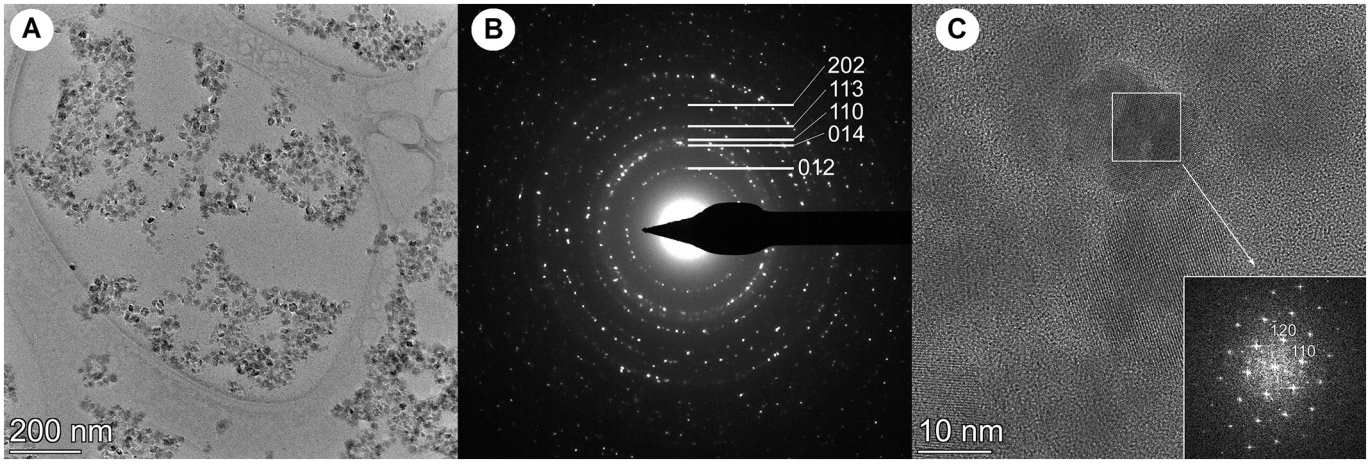

Fig. 1. (A) Low magnification transmission electron micrograph (A) and SAED pattern of the nanoparticles (B) of the NH colloid suspension. SAED pattern of the nanoparticles clearly indicates nanocrystalline haematite, Miller indices according to haematite structure are given for several of the innermost diffraction rings and (C) high resolution transmission electron micrograph of a nanoparticle with the insert showing the Fourier transform of the marked area. According to the Fourier transform, the nanoparticle is haematite viewed down the [001] zone axis.

supernatant contained a measurable amount of Fe as well (3.269 ± 0.096% of the total Fe content of the colloidal suspension). ^{57}Fe Mössbauer spectrum of the frozen ^{57}Fe-NH colloid suspension recorded at liquid nitrogen temperature (Fig. 2A) can be fitted with a model consisting of two paramagnetic quadrupole doublets, two magnetic sextets and a broad singlet (Gracheva et al., 2022).

3.2. Alterations in the physico-chemical properties by the interaction to plant roots

To enable a detailed analysis of the Fe species during the plant utilisation of the Fe content of the nanoparticles, Mössbauer spectrum of roots of dFe plants, supplied with ^{57}Fe-NH suspension of nominal Fe concentration of 100 μM for 30 min, was measured at low temperature

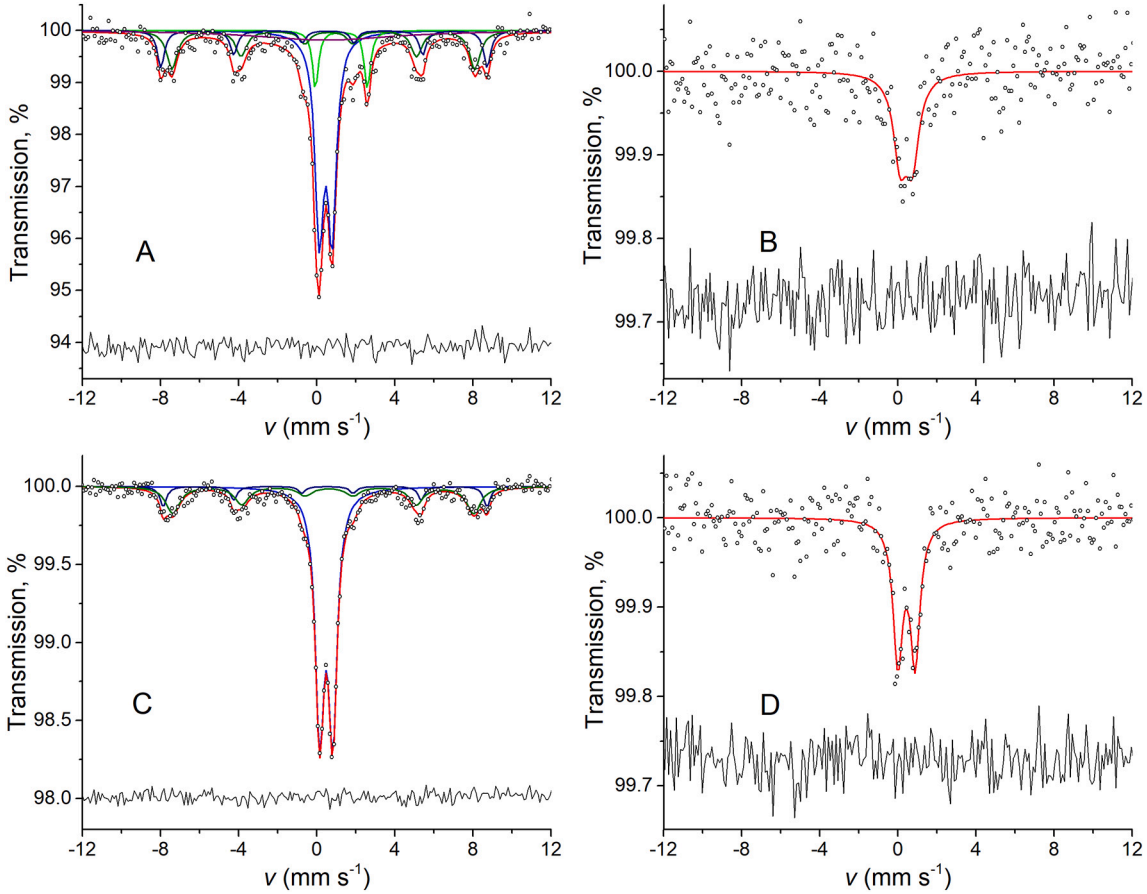

Fig. 2. Mössbauer spectra of (A) the frozen ^{57}Fe-NH colloid suspension sample, (B) dFe roots, supplied with ^{57}Fe-NH suspension of nominal Fe concentration of 100 μM for 30 min and (C) for one week, (D) dFe leaves, supplied with ^{57}Fe-NH suspension of nominal Fe concentration of 100 μM for one week.

($T = 80$ K). The spectrum exhibited one component with parameters ($\delta = 0.42(6)$ mm s^{-1}, $\Delta = 0.64(6)$ mm s^{-1}) typical for a high-spin Fe(III) in octahedral O_6 coordination (Fig. 2B). Nevertheless, the concentration of Fe in the sample was too small for a more precise identification of this component. The parameters of the observed component is, indeed, close to those of Fe(III)-citrate measured before by Kovács et al. (2009). No Fe (II) or magnetic components were detected.

Mössbauer spectrum of roots of dFe plants, supplied with ^{57}Fe-NH colloid suspension of nominal Fe concentration of 100 μM for one week, demonstrated the presence of two magnetic sextets and a paramagnetic doublet (Fig. 2C). The sextets have close hyperfine parameters to ones found in the initial suspension (Fig. 2A) corresponding to the original nanoparticles. The Fe(III) doublet has higher relative area (67%) than in the initial colloid suspension spectrum (41%). Due to the very similar Mössbauer parameters: Fe(III) in distorted O_6 octahedral coordination, this paramagnetic doublet component could not be further resolved. Important to underline, that neither Fe(II) components, nor relaxation singlet were observed in the spectrum of the roots.

TEM analysis revealed aggregates of electron dense particles in the middle lamellae between adjacent cell walls in NH treated but not in oFe samples (Fig. A2). Indeed, electron dense particles might have originated from the applied contrasting materials uranyl acetate and lead citrate. Thus, the samples were further analysed by HRTEM (Fig. 3A) and HAADF (Fig. 3C) and EDS elemental mapping (Fig. 3D and E). EDS revealed that abundance of both Fe and Pb (this latter originated from the contrasting material) was higher in the middle lamella between the adjacent cell walls across the root tip. In contrast to NH treated samples, accumulation of Fe was not observed neither in dFe nor in oFe plants (Figs. A3 and A4). According to analysis of EDS line profile crossing the cytoplasm, plasma membrane, cell wall and middle lamella regions of adjacent cells, an accumulation of Fe can be observed in the middle lamella between the adjacent cell walls in the NH treated samples (Fig. 3B), while in dFe and oFe roots no such sign in the Fe line profile was detected in the corresponding regions of the cells (Fig. A3B and A4B, where Fe Kα was identified as emission at 6.40 keV, Fig. A5). HRTEM analysis of NH treated roots indicates dense particles accumulating at the interfaces of the middle lamella and the adjacent walls (Fig. 4A–C), which corresponds to the linearly arranged high average atomic number particles observed on the HAADF images (Fig. 3C). HRTEM analysis revealed the presence of several, separate electron dense particles of few nanometres size in this region, which exhibit a clear crystalline structure (Fig. 4D). Based on the interplanar spacing values measured on the Fourier transforms, these nanoparticles can be unambiguously identified as haematite (Fig. 4E and F). Size analysis of the particles indicated a diameter of 1.96 ± 0.28 nm for the particles, where no particles were detected above the diameter of 2.85 nm (Fig. A1B,D,F). Size distribution in the NH colloid suspension and in the biological matrix (middle lamella of the root tip cell walls) was compared by Mann-Whitney test

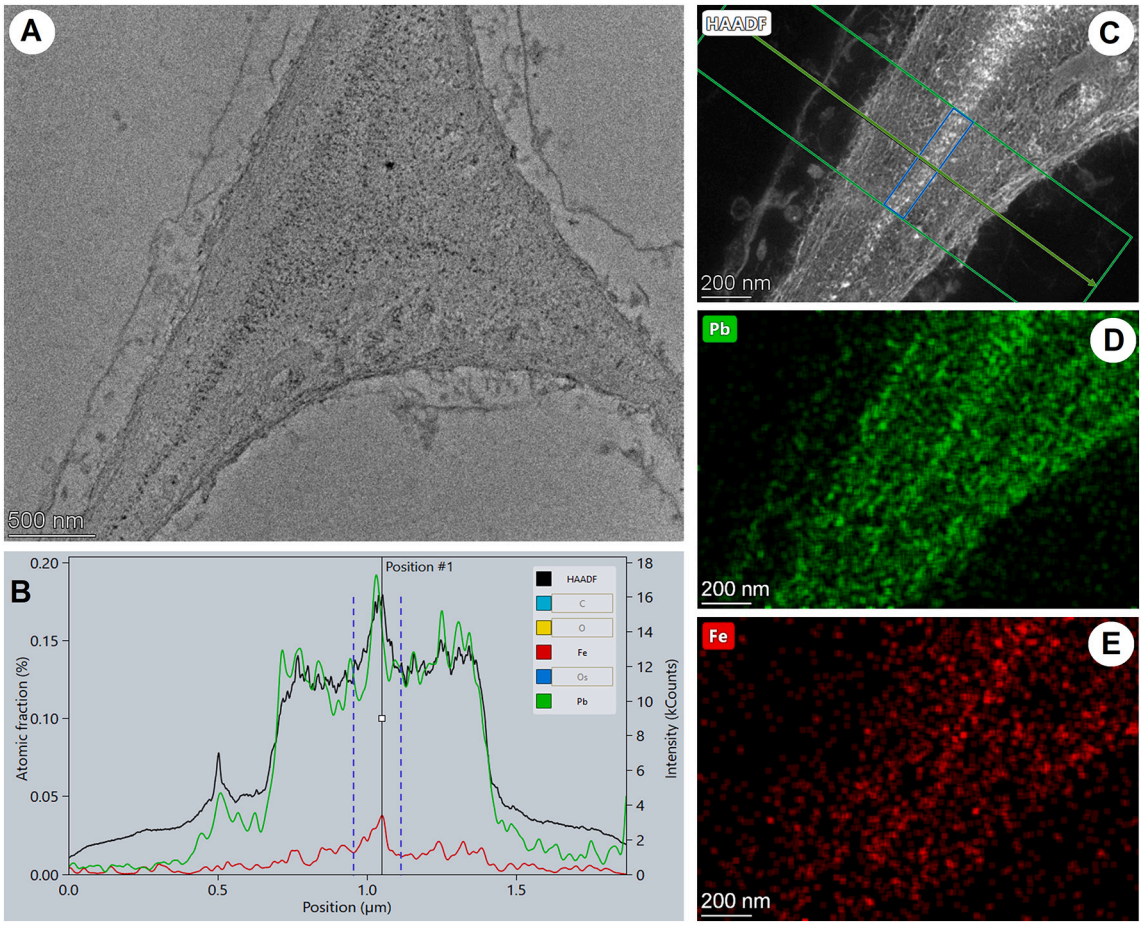

Fig. 3. Transmission electron micrograph of a three-cell junction (A) and high-angle annular dark-field (HAADF) image (C) of the root tip meristem cells of NH treated plants. Energy dispersive X-ray spectroscopy (EDS) line profile analysis (B) performed by merging data applying a 300 pixel integration width perpendicular to the line indicated on (C). Elemental distribution maps of Pb as for contrasting material (D) and Fe (E) was created based on the Pb $L\alpha_1$ and Fe Kα peaks (10.55 and 6.40 keV, respectively). Area of the line profile between dashed lines on (B) is the region marked by blue box on (C), which coincides with the middle lamella in the two-cell junction. In this area large number of high atomic number particles (bright spots) are seen, and, according to EDS line profile analysis, besides the contrasting material Pb, is characterized by elevated concentration of Fe. (For interpretation of the references to colour in this figure legend, the reader is referred to the web version of this article.)

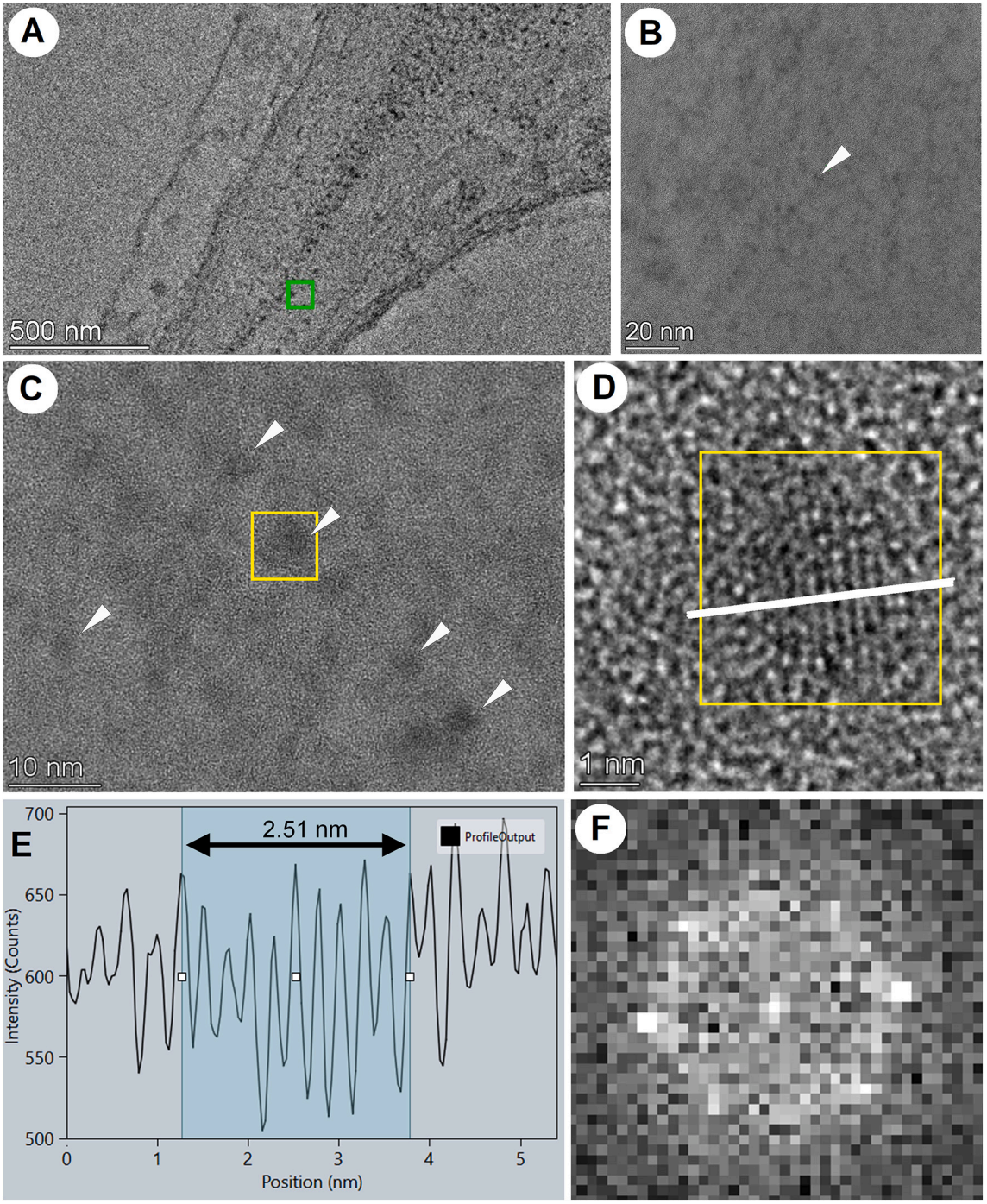

Fig. 4. High-resolution transmission electron micrographs (HRTEM; A–C) of the root tip meristem cells of NH treated plants. Subdivision B is a high-resolution site indicated by a green square on subdivision A (sample is identical to 3A). Bar on (A) equal to 500 nm. Electron dense particles, pointed by arrowheads, accumulated in the middle lamella of the cell wall at two-cell junctions. HRTEM indicate the presence of several separate electron dense particles (C). Atomic resolution image of an individual particle proves crystalline structure (D), the measured periodicity is 2.51 nm, typical to haematite d(110) interplanar spacing (E). Fourier transform support unambiguously haematite nanoparticle in [001] zone axis orientation (F). (For interpretation of the references to colour in this figure legend, the reader is referred to the web version of this article.)

(Table A2) indicating a strong significant different among the size of the particle populations. Since no overlapping was detected between the minimum particle size in the NH colloid suspension and the maximum size of particles in the biological matrix, the particle populations were considered to be distinct. Therefore, particles detected in the middle lamella region suggested to have been underwent a massive reduction in their size while accumulating in the roots.

3.3. Suppression of iron deficiency responses

CsFRO genes encoding root plasma membrane ferric chelate reductases and *CsRIBA1* encoding for GTP cyclohydrolase II, involved in riboflavin synthesis showed a circadian rhythm in their expression in dFe plants (Figs. 5 and 6). In the expression pattern of the genes of interest (GOI), a morning and an evening peaks were identified, among which the relative transcript amount was found generally lower at the

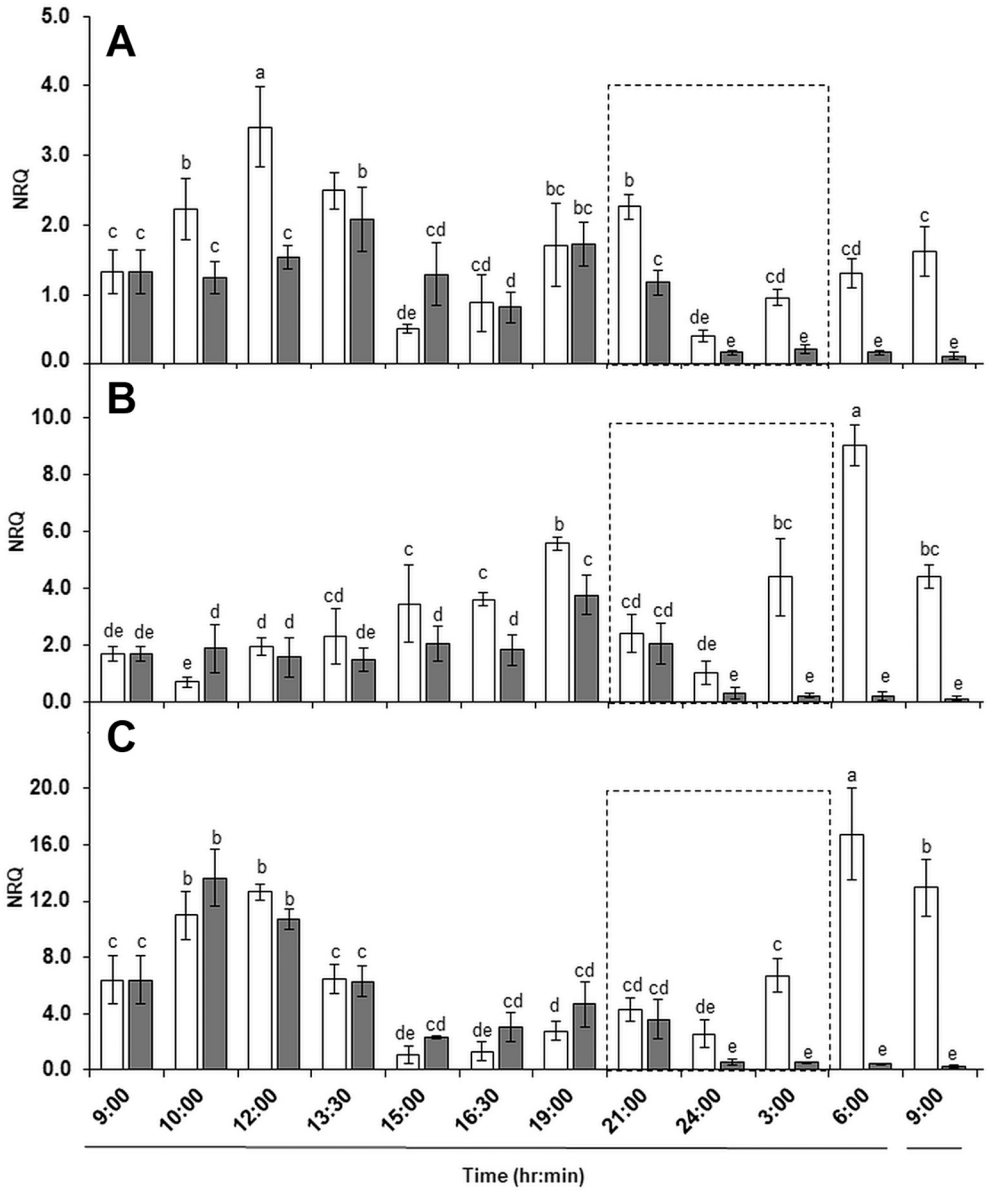

Fig. 5. Changes in the relative transcript amount of *CsFRO1* (A), *CsFRO3* (B) and *CsRIBA1* (C) in iron deficient (dFe, open columns) and in NH treated (grey columns) during the time of treatment. The recovery treatment started at 9:00 am on the first day. Values are also normalised on the basis of the relative transcript amount measured at 9:00 am on plants grown continuously on 10 μM Fe(III)-EDTA. Dark period is shown by dashed line square. Days of treatment are illustrated below the scale for time of treatment by broken line. Error bars represent SD values. To compare the differences, one-way ANOVA was performed with Tukey-Kramer *post-hoc* tests on the treatments ($P < 0.01$; $n = 4 \times 3$ [biological×technical]).

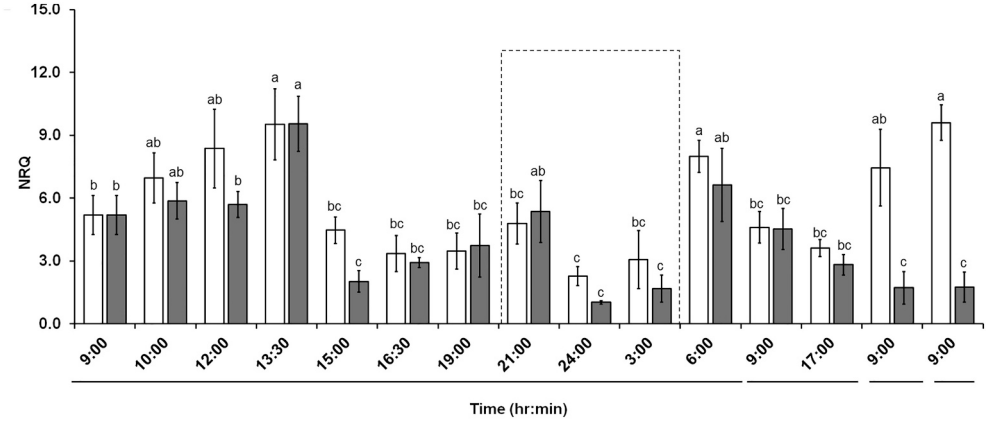

Fig. 6. Changes in the relative transcript amount of *CsFRO2* in iron deficient (dFe, open columns) and in NH treated (grey columns) during the time of treatment. The recovery treatment started at 9:00 am on the first day. Values are also normalised on the basis of the relative transcript amount measured at 9:00 am on plants grown continuously on 10 μM Fe(III)-EDTA. Dark period is shown by dashed line square. Days of treatment are illustrated below the scale for time of treatment by broken line. Error bars represent SD values. To compare the differences, one-way ANOVA was performed with Tukey-Kramer *post-hoc* tests on the treatments ($P < 0.01$; $n = 4 \times 3$ [biological × technical]).

evening peak than that at the morning peak. In oFe plants, the expression of GOIs was at the detection limit at all time points without any significant periodicity.

NH treatment affected Fe deficiency response genes differentially. As for the first sign of the effect of NH treatment the morning increase in the expression of *CsFRO1* was delayed compared to the corresponding dFe plants (Fig. 5A). In addition, the evening rise was also broken after 19:00 pm and it started to decrease thereafter to a minimum at 24:00 pm. Furthermore, the morning increase was completely vanished on the next day and relative transcript amount of *CsFRO1* further remained in the range of oFe plants. Thus, elimination of the Fe deficiency induced expression of *CsFRO1* required 15 h in total from the beginning of the recovery treatment. Similar to *CsFRO1*, the relative transcript amount of *CsFRO3* also got decreased after 15 h of treatment, which resulted in the vanished morning peak (Fig. 5B). Similar to the expression of *CsFRO1&3*, that of *CsRIBA1* also reacted in 15 h in response to NH treatment: the morning peak in the expression vanished on the second day of treatment (Fig. 5C). Although relative transcript amount of *CsFRO2* was also affected by NH treatment (Fig. 6), the suppression in the expression of *CsFRO2* was significantly delayed in time compared to that of *CsFRO1&3*. In consequence, the relative transcript amount of *CsFRO2* remained unaltered compared to dFe plants both in extent and in the rhythm of change in the first 24 h of NH treatment and only decreased after 48 h of the treatment. In consequence, the pattern of expression of *CsFRO1&3* and *CsRIBA1* and the response of their relative transcript amounts to NH treatment shared high similarities, but all these for *CsFRO2* proved to be distinct.

3.4. Analysis of CsFRO2 protein sequence

Since the response in the relative transcript amount of *CsFRO2* to NH treatment proved to be distinct than that of *CsFRO1&3* and *CsRIBA1* we questioned that *CsFRO2* encode a root ferric chelate reductase enzyme. Although protein sequence analysis of Marastoni et al. (2019) indicated that OsFRO1, and MtFRO2&5 are the closest alignments to CsFRO2, all associated with root FCR activity, tblastn analysis of CsFRO2 sequence against *Arabidopsis* database indicated AtFRO7 (chloroplastidial) with the highest score (Appendix B). Protein sequence alignment of CsFRO2 on AtFRO2, OsFRO1 and AtFRO7 indicated higher similarities between CsFRO2 and AtFRO7 than between CsFRO2 and OsFRO1 (Figs. A7–A8). In the translated protein sequence of CsFRO2, a 20 amino acid long cut-off signal peptide was identified (Fig. A9). Signal peptide analysis indicated a targeting to the secretory system with the highest score, whereas mitochondrial and plastidial targeting has not been excluded (Fig. A10). In conclusion, CsFRO2 was identified as a member of the intracellular Fe homeostasis in *Cucumis sativus*.

3.5. Suppression of ferric chelate reductase activity of roots

The dFe conditions resulted in a significantly increased ferric chelate reductase (FCR) activity of roots compared to that of in oFe plants. FCR activity of roots also showed circadian rhythmicity with peak activities in the morning and in the evening (Fig. 7). FCR activity of oFe plants was below the detection limit. NH treatment did not induce significant alterations in the FCR activity from that of the dFe plants during the first day of treatment and decreased FCR activity was first recorded 24 h after the initiation of the NH treatment with the disruption in the morning peak (Fig. 7). A continuous decline in the FCR activity finally led to the elimination of the afternoon peak on the second day. FCR activity of NH treated plants was finally eliminated by the third day of the treatment (relaxing required 48 h). Thus, the recovery of the FCR activity was delayed from the suppression in the relative transcript amounts of *CsFRO1&3* and *CsRIBA1*.

3.6. Iron translocation to the foliage

NH treatment induced a significant increase in the SPAD value (representing chlorophyll content) of the leaves of the treated plants (Fig. A6) indicating the utilisation and translocation of Fe. To detect traces of NH translocation to the aerial tissues, leaves of NH treated plants were subjected to analysis. Mössbauer spectrum of the leaves of the regenerated plants (Fig. 2D) shows a symmetric doublet with parameters $\delta = 0.43(2)$ mm s^{-1}, $\Delta = 0.88(3)$ mm s^{-1} corresponding to high-spin Fe(III). Since the relative line width of the doublet is rather large, the obtained spectrum is probably a composition of several doublets corresponding to different microenvironments with close hyperfine parameters. However, the concentration of Fe and, consequently, the quality of the spectrum is too low for precise distinguishing of these species. The average quadrupole splitting of the doublet is significantly higher than one observed in the original suspension or in the roots. This increase can be explained by the fact that the applied ^{57}Fe was partly incorporated to Fe_4S_4 proteins ($\delta = 0.46$ mm s^{-1}, $\Delta = 1.06$ mm s^{-1}, according to Solti et al., 2016) which represent a significant amount of Fe content in chloroplasts.

4. Discussion

Cucumber plants treated by NH colloid suspension exhibited sufficient regeneration from Fe deficiency. Similar to our results, multiple studies indicated that plants are able to take up Fe containing nanoparticles. In *Citrus reticulata*, γ-Fe_2O_3 of 21.2 ± 2.9 nm particle size were shown to be taken up and migrate to the vascular bundle without any signs of translocation (Li et al., 2017). However, particle size seems to be a highly limiting factor of nanoparticle utilisation. Marusenko et al. (2013) reported that *Arabidopsis thaliana* plants are unable to utilise the

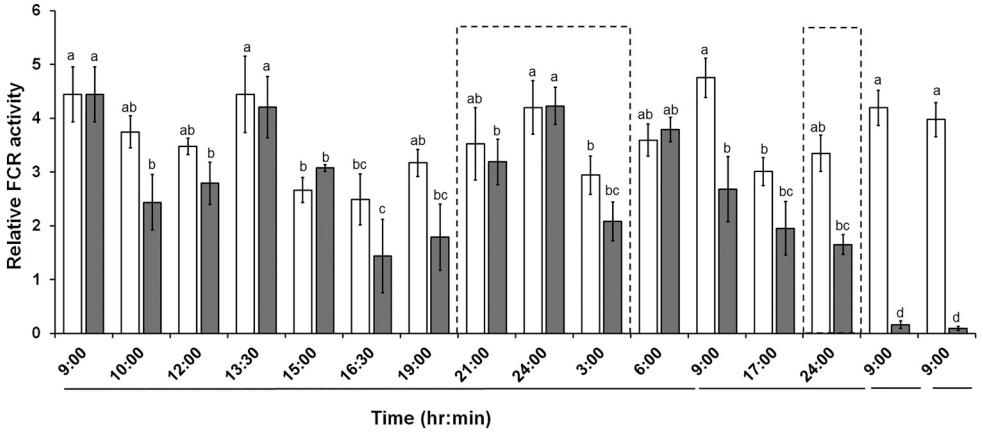

Fig. 7. Changes in the ferric chelate reductase activity in iron deficient (dFe, open columns) and in NH treated (grey columns) during the time of treatment. The recovery treatment started at 9:00 am on the first day. Values are also normalised on the basis of the values measured at 9:00 am on plants grown continuously on 10 μM Fe(III)-EDTA (5.2 ± 2.0 nmol Fe g^{-1} fw min^{-1}). Dark periods are shown by dashed line square. Days of treatment are illustrated below the scale for time of treatment by broken line. Error bars represent SD values. To compare the differences, one-way ANOVA was performed with Tukey-Kramer *post-hoc* tests on the treatments ($P < 0.01$; $n = 4 \times 3$ [biological×technical]).

Fe content of α-Fe_2O_3 nanoparticles of 22.3–67.0 nm particle size. Yuan et al. (2018) reported that zero valent Fe nanoparticles are absorbed and transported to the central cylinder in the roots of *Capsicum anuum*, but the way of transportation was apoplastic. Although in our study we could have not detected any NH particles in the aerial tissues, and ^{57}Fe Mössbauer spectroscopy indicated a composition of different microenvironments with close hyperfine parameters, we cannot exclude the possibility of the translocation of NH particles to the shoot. Iannone et al. (2021) reported that citric acid coated Fe_3O_4 (magnetite) NPs are not translocated to the aerial parts in soybean (*Glycine* max) and only scarcely in alfalfa (*Medicago sativa*). Tombuloglu et al. (2020a) found, however, that Fe_3O_4 can penetrate into the phloem in pumpkin (*Cucurbita maxima*) indicating a translocation of the nanoparticles towards the aerial tissues. Using confocal microscopy, Al-Amri et al. (2020) found in wheat (*Triticum aestivum*) that Fe_2O_3 nanoparticles cause damages in the cells of the root tip without macroscopic effects. Vibrating sample magnetometer analysis data suggested that Fe_2O_3 nanoparticles were translocated to the leaves in wheat. Similarly, magnetic signals also suggest, that α-Fe_2O_3 nanoparticles are translocated to the leaves in barley (*Hordeum vulgare*) (Tombuloglu et al., 2020a, 2020b). Although in monocots, translocation of α-Fe_2O_3 nanoparticles seems to be general, data on dicot models is still scarce. The translocation of Fe containing nanoparticles among angiosperms, indeed, seems to be rather taxon-specific. Regardless on the translocation Fe containing nanoparticles to the aerial tissues, the majority of the nanoparticles seem to be dismantled in the roots.

The interaction between nanoparticles and plant tissues is also affected by the properties of the apoplast. The size exclusion limit of the cell wall of plants is assumed to be in the range of 5–20 nm (Schwab et al., 2016; Ma and Yan, 2018; Lv et al., 2019; Wang et al., 2019). Nevertheless, based on taxon and developmental stage based differences, Kurczyńska et al. (2021) indicated that the size exclusion limit of the apoplast can be as low as 1.6–4.6 nm. Our HRTEM and EDS analysis revealed that NH particles were unable to enter the symplast of the cells in their intact form but accumulated in the middle lamella in the apoplast. Since the size of the Fe containing particles was significantly reduced compared to the original suspension (10–20 nm *versus* ~ 2.5 nm), release of Fe from the particles is proven. Although the exact locus of the release cannot be revealed, a direct interaction between plasma membrane FRO proteins and the Fe containing nanoparticles is excluded. Therefore, utilisation of the Fe content of the NH is an action remote of the plasma membrane. Mössbauer spectroscopy results revealed changes in the abundance ratio of different Fe components reflecting the mobilisation of Fe from nanoparticles. Although the applied surfactant (PEG) also perform a reducing capacity, and thus PEG might have induced interfacial electron transfer to structural Fe(III), resulted in the formation of facilitated the formation of goethite and δ-FeOOH (ferroxyhyte, a highly disordered structural variant of haematite) (Gracheva et al., 2022). Thus, the presence of PEG do not acceletared the formation of dissolved Fe but rather initiated the formation of an oxide mixture on the surface of the nanoparticles. Therefore, the dissolution of Fe is a process that is independent of the applied surfactant.

Although in 30 min of NH treatment, no magnetic components were detected in the spectrum, suggesting that the time was too short for the nanoparticles to be attached or utilised, longer incubation with NH revealed that nanoparticles formed a non-washable pool in the root apoplast where the basic physico-chemical features remained unchanged. Indeed, the component of paramagnetic doublet may not only be associated with particles attached to the roots or infiltrate the apoplast but also with Fe of biological incorporation after a transmembrane uptake. In contrast to the Fe(II) accumulation observed in Fe deficient plants short after supplying them with Fe(III)-citrate or Fe(III)-EDTA in high concentration (Kovács et al., 2016), roots exhibited no detectable amount of Fe(II), indicating that the mobilisation of Fe from NH has significantly lower rate. Apoplast mobilisation of Fe from NH is exclusive since neither Fe containing nanoparticles were found in the symplast, nor haematite related species were detected in the leaves. In conclusion, translocation of NH towards the shoots is unlikely. Thus, regeneration of Fe deficiency induced symptoms is based on the apoplast liberation of Fe from NH particles.

Cucumber is a flavin secreting Strategy I dicot releasing among other 4′-ketoriboflavin (Satoh et al., 2016) as Fe deficiency response, together with the increased expression of *FRO*s. Riboflavin derivatives are suggested to contribute to the reduction of Fe(III) operating as reducing power shuttles (Welkie, 2000; Sisó-Terraza et al., 2016; Gheshlaghi et al., 2021) and thus collaborate in the ferric reduction. Regarding induction of Fe deficiency responses, Connolly et al. (2002, 2003) reported that when *Arabidopsis* plants are transferred to an Fe free medium, transcripts of both *IRT1* and *FRO2* became detectable in 24 h, whereas the peak in the relative transcript amount was found on the 3rd day of treatment. Suppression of Fe deficiency induced responses requires a similar time frame in *Arabidopsis*: Vert et al. (2003) reported that after supplying Fe deficient plants with 500 μM Fe(III)-EDTA, expression of *IRT1* and *FRO2* decreases to a minimum in 24 h and zero in 48 h. In cucumber, three genes have been previously associated to root plasma membrane ferric chelate reductase activity (Waters et al., 2014; Marastoni et al., 2019). Nevertheless, response to NH treatment varied among these *CsFRO*s. Although the expression of *CsFRO1&3* vanished in 24 h, that of *CsFRO2* only decreased in 48 h. Since in the translated protein sequence of CsFRO2 we identified a signal peptide that directs the protein into intracellular membranes, we concluded that CsFRO2 is not involved in the root FCR activity and represents a member of the intracellular Fe homeostasis. In consequence, suppression of the elevated transcript amount of *CsFRO2* indicates the restoration of the optimum Fe homeostasis on cucumber root cells.

Together with *CsFRO1&3* genes, the expression of riboflavin biosynthesis element *CsRIBA1*, catalysing the initial step of riboflavin biosynthesis (Hedtke et al., 2012; Hiltunen, 2016), increased in response to Fe deficiency, in accordance with Rodríguez-Celma et al. (2013) and Hsieh and Waters (2016). The parallel suppression of *CsRIBA1* to *CsFRO1&3* underlines that regulations of root FCR activity and flavin biosynthesis are coordinated and thus flavin biosynthesis is an inclusive Fe deficiency response in cucumber. Ectopically expressed *Arabidopsis bHLH*s in tobacco (*Nicotiana tabacum*) caused Fe deficiency-independent flavin secretion (Vorwieger et al., 2007). Hsieh and Waters (2016) reported a complete abolishment of *CmRIBA1* in *fefe* mutant which lacks *Cucumis* Fe deficiency response bHLH (analogous in function with AtbHLH38/39). Altogether these data suggest that secretion of riboflavin derivatives stay under control of core Fe deficiency signalling. In *Arabidopsis*, Fe binding of haemerythrin domain proteins Brutus and Brutus-like 1&2 leads to the elimination of IVc class bHLH transcription factors (Schwarz and Bauer, 2020; Rodríguez-Celma et al., 2019). Although the cellular sensing of Fe has not been revealed in other dicots, homologous mechanism is supposed to exist in cucumber. Fe deficiency response genes also stay under the regulation of the circadian rhythm (Xu et al., 2019) as we also proved in regard with *CsFRO*s and *CsRIBA1*. In *Arabidopsis*, expression of both *AtFER2* and *AtIRT1* showed a clear dependency on the light periods (Xu et al., 2019). Vert et al. (2003) showed that both *AtIRT1* and *AtFRO2* express during the diurnal periods in *Arabidopsis*. Hong et al. (2013) confirmed that the mRNA accumulation of *AtIRT1*, *AtbHLH39* and *AtFERRITIN* (*FER*) *1* is regulated by the circadian clock in *Arabidopsis*. In consequence, both in the NH treatment caused suppression and circadian rhythmicity in the relative transcript amount of *CsFRO1&3* and *CsRIBA1* the role of Fe signalling is proposed.

FCR activity of roots generally followed the rhythmicity of the expression of *CsFRO1&3* and *CsRIBA1* genes. Since variations in the FCR activity caused by the circadian rhythm highly overlaps with NH treatment induced changes, effect should be taken into account by interpreting any physiological measurements on the recovery of Fe deficiency. López-Millán et al. (2001) reported that 24 h after resupply of 45 μM Fe EDTA to Fe deficient sugar beet (*Beta vulgaris*) plants only

resulted in a 15–20% decrease in FCR activity whereas some more 70–80% decrease was recorded in 96 h of Fe resupply. Pestana et al. (2012) also reported the slow decrease of FCR activity upon providing 10 μM Fe(III)-EDDHA to Fe deficient strawberry (*Fragaria* × *ananassa*) roots. In comparison, we recorded a decrease in the FCR activity at 97 and 98% in 48 and 72 h after starting the NH treatment, respectively. Since suppression of the FCR activity delayed compared to the decrease in the relative transcript amount of *CsFRO1&3 and CsRIBA1* as response to NH treatment, post-translational suppression and removal of functionally active plasma membrane FRO enzymes require a longer time / stay under distinct regulation pathway. Post-translational regulation of root plasma membrane FROs collaborates in the elimination of root FCR activity (Pan et al., 2015). Martín-Barranco et al. (2020) indicated that ubiquitination of AtFRO2 is an important post-translational modification in the inactivation of root FCR activity that resulted in degradation or *in situ* suppression of the activity in *Arabidopsis*. In conclusion, the suppression of root FCR activity proposed by ubiquitination in response to increased bioavailability of Fe require approximately 48 h. This suppression contributes in the avoidance of inducing Fe toxicity by liberating excess Fe from the insoluble sources.

5. Conclusion

Taken together, accumulation of NH particles in the root apoplast and decrease in size of particles supports the gradual release of Fe from NH. Since no direct contacts were found between the particles and plant plasma membranes (plasma membrane localized FROs) and the fact that NH particles are resistant against low pH, the reducing power shuttle operated by flavins is suggested to be involved in the Fe liberation from NH particles. Inclusivity of this shuttle mechanism in Fe deficiency responses is also supported by the parallel suppression of flavin biosynthesis and plasma membrane ferric chelate reductases. The parallel alterations in the relative transcript amount of *CsFRO1&3* and *CsRIBA1* both in the circadian rhythm and in the NH treatment response suggest a direct control of bHLH type transcription factor FeFe over the general Fe deficiency responses in cucumber. Fe deficiency responses have a clear circadian rhythmicity that has a high importance at addressing physiological measurements on root FCR activity.

Author contribution

ÁS and ZK designed and supervised the study. NH suspension was fabricated by GT. Transmission electron microscopy investigation of the nanocolloid suspension and STEM-EDS analyses were carried out by VKK. Physico-chemical properties were evaluated by ZK. Particle size analysis was performed by AS, VKK and ÁS. Elemental analyses were performed by ZM. Mössbauer spectroscopy analysis was performed by MG, KK and ZH. Sedimentation studies were performed by KK and ÁS. Transmission electron microscopy studies were performed by VKK, ÁK and FP. Bioinformatics was applied by AS and ÁS. Expression analysis studies were performed by AS, WA and MS-K. Ferric chelate reductase studies were performed by AS, BM and FF. AS, MG, VKK, ÁK, ZK, KK and ÁS wrote and all authors critically reviewed the manuscript.

Funding

This work was supported by the grants financed by the National Research, Development and Innovation Office, Hungary (NKFIH K-124159; K-115913 and VEKOP-2.3.3-15-2016-00008). This work was completed as part of the ELTE Thematic Excellence Programme 2020 supported by the National Research, Development and Innovation Office (TKP2020-IKA-05). The transmission electron microscopy facility at the Centre for Energy Research was granted by the European Structural and Investment Funds (VEKOP-2.3.3-15-2016-00002). V.K.K. was supported by the János Bolyai Postdoctoral Fellowship of the Hungarian Academy of Sciences (367/17) and the ÚNKP-19-4 New National Excellence Program of the Ministry for Innovation and Technology, Hungary. M S-K was supported by the New National Excellence Program of the Ministry of Human Capacities, Hungary (ÚNKP-20-3-I-862).

CRediT authorship contribution statement

Amarjeet Singh: Investigation, Data curation, Writing – original draft, Writing – review & editing, Visualization. **Maria Gracheva:** Investigation, Writing – original draft, Writing – review & editing, Visualization. **Viktória Kovács Kis:** Investigation, Writing – original draft, Writing – review & editing, Visualization, Funding acquisition. **Áron Keresztes:** Investigation, Writing – review & editing. **Máté Sági-Kazár:** Investigation, Writing – review & editing, Funding acquisition. **Brigitta Müller:** Investigation, Writing – review & editing. **Fruzsina Pankaczi:** Investigation, Writing – review & editing. **Waqas Ahmad:** Investigation, Writing – review & editing. **Krisztina Kovács:** Investigation, Writing – original draft, Writing – review & editing. **Zoltán May:** Investigation, Writing – review & editing. **Gyula Tolnai:** Methodology, Resources, Writing – review & editing. **Zoltán Homonnay:** Methodology, Resources, Investigation, Writing – review & editing, Funding acquisition. **Ferenc Fodor:** Methodology, Resources, Investigation, Writing – review & editing, Funding acquisition. **Zoltán Klencsár:** Conceptualization, Supervision, Methodology, Resources, Investigation, Writing – original draft, Writing – review & editing, Project administration, Funding acquisition. **Ádám Solti:** Conceptualization, Supervision, Methodology, Resources, Investigation, Data curation, Writing – original draft, Writing – review & editing, Visualization, Project administration, Funding acquisition.

Declaration of Competing Interest

All authors state that there is no conflict of interest in relation with the present work.

Data availability

All datasets generated for this study are included in the article/ appendices, further inquiries can be directed to the corresponding author.

Acknowledgements

We would like to thank Csilla Gergely for sample preparation for transmission electron microscopy on biological samples and Sándorné Pardi for the assistance to the molecular laboratory work.

Supplementary data

Supplementary data to this article can be found online at https://doi.org/10.1016/j.impact.2022.100444.

References

Al-Amri, N., Tombuloglu, H., Slimani, Y., Akhtar, S., Barghouthi, M., Almessiere, M., Alshammari, T., Baykal, A., Sabit, H., et al., 2020. Size effect of iron (III) oxide nanomaterials on the growth, and their uptake and translocation in common wheat (*Triticum aestivum* L.). Ecotoxicol. Environ. Saf. 194, 110377 https://doi.org/10.1016/j.ecoenv.2020.110377.

Colombo, C., Palumbo, G., He, J.Z., Pinton, R., Cesco, S., 2014. Review on iron availability in soil: interaction of Fe minerals, plants, and microbes. J. Soils Sediments 14, 538–548. https://doi.org/10.1007/s11368-013-0814-z.

Connolly, E.L., Fett, J.P., Guerinot, M.L., 2002. Expression of the IRT1 metal transporter is controlled by metals at the levels of transcript and protein accumulation. Plant Cell 14, 1347–1357. https://doi.org/10.1105/tpc.001263.

Connolly, E.L., Campbell, N.H., Grotz, N., Prichard, C.L., Guerinot, M.L., 2003. Overexpression of the FRO2 ferric chelate reductase confers tolerance to growth on low iron and uncovers posttranscriptional control. Plant Physiol. 133, 1102–1110. https://doi.org/10.1104/pp.103.025122.

Gao, F., Dubos, C., 2021. Transcriptional integration of plant responses to iron availability. J. Exp. Bot. 72, 2056–2070. https://doi.org/10.1093/jxb/eraa556.

Gheshlaghi, Z., Luis-Villarroya, A., Álvarez-Fernández, A., Khorassani, R., Abadía, J., 2021. Iron deficient *Medicago scutellata* grown in nutrient solution at high pH accumulates and secretes large amounts of flavins. Plant Sci. 303, 110664 https://doi.org/10.1016/j.plantsci.2020.110664.

Gracheva, M., Klencsár, Z., Kovács Kis, V., Béres, K.A., May, Z., Halasy, V., Singh, A., Fodor, F., Solti, Á., et al., 2022. Iron nanoparticles for plant nutrition: synthesis, transformation and utilization by the roots of *Cucumis sativus*. J. Mater. Res. https://doi.org/10.1557/s43578-022-00686-z.

Hedtke, B., Alawady, A., Albacete, A., Kobayashi, K., Melzer, M., Roitsch, T., Masuda, T., Grimm, B., 2012. Deficiency in riboflavin biosynthesis affects tetrapyrrole biosynthesis in etiolated *Arabidopsis* tissue. Plant Mol. Biol. 78, 77–93. https://doi.org/10.1007/s11103-011-9846-1.

Hiltunen, H.M., 2016. Functional analysis of RIBA, the introductory enzyme for riboflavin biosynthesis. PhD thesis, Humboldt-Universität zu Berlin, Lebenswissenschaftliche Fakultät. https://edoc.hu-berlin.de/handle/18452/18177.

Hong, S., Kim, S.A., Guerinot, M.L., McClung, C.R., 2013. Reciprocal interaction of the circadian clock with the iron homeostasis network in *Arabidopsis*. Plant Physiol. 161, 893–903. https://doi.org/10.1104/pp.112.208603.

Hsieh, E.J., Waters, B.M., 2016. Alkaline stress and iron deficiency regulate iron uptake and riboflavin synthesis gene expression differently in root and leaf tissue: implications for iron deficiency chlorosis. J. Exp. Bot. 67, 5671–5685. https://doi.org/10.1093/jxb/erw328.

Iannone, M.F., Groppa, M.D., Zawoznik, M.S., Coral, D.F., van Raap, M.B.F., Benavides, M.P., 2021. Magnetite nanoparticles coated with citric acid are not phytotoxic and stimulate soybean and alfalfa growth. Ecotoxicol. Environ. Saf. 211, 111942 https://doi.org/10.1016/j.ecoenv.2021.111942.

Jang, J.H., Dempsey, B.A., Burgos, W.D., 2007. Solubility of hematite revisited: effects of hydration. Environ. Sci. Technol. 41, 7303–7308. https://doi.org/10.1021/es070535t.

Koochana, P.K., Mohanty, A., Parida, A., Behera, N., Behera, P.M., Dixit, A., Behera, R.K., 2021. Flavin-mediated reductive iron mobilization from frog M and mycobacterial ferritins: impact of their size, charge and reactivities with NADH/O_2. JBIC J. Biol. Inorg. Chem. 26, 265–281. https://doi.org/10.1007/s00775-021-01850-2.

Kovács, K., Kuzmann, E., Tatár, E., Vértes, A., Fodor, F., 2009. Investigation of iron pools in cucumber roots by Mössbauer spectroscopy: direct evidence for the strategy I iron uptake mechanism. Planta 229, 271–278. https://doi.org/10.1007/s00425-008-0826-x.

Kovács, K., Pechoušek, J., Machala, L., Zbořil, R., Klencsár, Z., Solti, Á., Tóth, B., Müller, B., Pham, H.D., Kristóf, Z., et al., 2016. Revisiting the iron pools in cucumber roots: identification and localization. Planta 244, 167–179. https://doi.org/10.1007/s00425-016-2502-x.

Krämer, S.M., Crowley, D.E., Kretzschmar, R., 2006. Geochemical aspects of phytosiderophore-promoted iron acquisition by plants. Adv. Agron. 91, 1–46. https://doi.org/10.1016/S0065-2113(06)91001-3.

Kurczyńska, E., Godel-Jędrychowska, K., Sala, K., Milewska-Hendel, A., 2021. Nanoparticles - plant interaction: what we know, where we are? Appl. Sci. 11, 5473. https://doi.org/10.3390/app11125473.

Lemanceau, P., Bauer, P., Krämer, S., Briat, J.F., 2009. Iron dynamics in the rhizosphere as a case study for analyzing interactions between soils, plants and microbes. Plant Soil 321, 513–535. https://doi.org/10.1007/s11104-009-0039-5.

Li, J., Hu, J., Xiao, L., Gan, Q., Wang, Y., 2017. Physiological effects and fluorescence labeling of magnetic iron oxide nanoparticles on citrus (*citrus reticulata*) seedlings. Water Air Soil Pollut. 228, 1–9. https://doi.org/10.1007/s11270-016-3237-9.

López-Millán, A.F., Morales, F., Gogorcena, Y., Abadía, A., Abadía, J., 2001. Iron resupply-mediated deactivation of Fe-deficiency stress responses in roots of sugar beet. Funct. Plant Biol. 28, 171–180. https://doi.org/10.1071/PP00105.

Lv, J., Christie, P., Zhang, S., 2019. Uptake, translocation, and transformation of metal-based nanoparticles in plants: recent advances and methodological challenges. Environ. Sci. Nano 6, 41–59. https://doi.org/10.1039/C8EN00645H.

Ma, X., Yan, J., 2018. Plant uptake and accumulation of engineered metallic nanoparticles from lab to field conditions. Curr. Opin. Environ. Sci. Health 6, 16–20. https://doi.org/10.1016/j.coesh.2018.07.008.

Marastoni, L., Pii, Y., Maver, M., Valentinuzzi, F., Cesco, S., Mimmo, T., 2019. Role of *Azospirillum brasilense* in triggering different Fe chelate reductase enzymes in cucumber plants subjected to both nutrient deficiency and toxicity. Plant Physiol. Biochem. 136, 118–126. https://doi.org/10.1016/j.plaphy.2019.01.013.

Marshall, T.A., Morris, K., Law, G.T., Livens, F.R., Mosselmans, J.F.W., Bots, P., Shaw, S., 2014. Incorporation of uranium into hematite during crystallization from ferrihydrite. Environ. Sci. Technol. 48, 3724–3731. https://doi.org/10.1021/es500212a.

Martín-Barranco, A., Spielmann, J., Dubeaux, G., Vert, G., Zelazny, E., 2020. Dynamic control of the high-affinity iron uptake complex in root epidermal cells. Plant Physiol. 184, 1236–1250. https://doi.org/10.1104/pp.20.00234.

Marusenko, Y., Shipp, J., Hamilton, G.A., Morgan, J.L.L., Keebaugh, M., Hill, H., Dutta, A., Zhuo, X., Upadhyay, N., et al., 2013. Bioavailability of nanoparticulate hematite to *Arabidopsis thaliana*. Environ. Pollut. 174, 150–156. https://doi.org/10.1016/j.envpol.2012.11.020.

Matijević, E., 1985. Production of monodispersed colloidal particles. Annu. Rev. Mater. Sci. 15, 483–516. https://doi.org/10.1146/annurev.ms.15.080185.002411.

Mihailova, G., Solti, Á., Sárvári, É., Keresztes, Á., Rapparini, F., Velitchkova, M., Simova-Stoilova, L., Aleksandrov, V., Georgieva, K., 2020. Freezing tolerance of photosynthetic apparatus in the homoiochlorophyllous resurrection plant *Haberlea rhodopensis*. Environ. Exp. Bot. 178, 104157 https://doi.org/10.1016/j.envexpbot.2020.104157.

Mimmo, T., Del Buono, D., Terzano, R., Tomasi, N., Vigani, G., Crecchio, C., Pinton, R., Zocchi, G., Cesco, S., 2014. Rhizospheric organic compounds in the soil-microorganism-plant system: their role in iron availability. Eur. J. Soil Sci. 65, 629–642. https://doi.org/10.1111/ejss.12158.

Müller, B., Kovács, K., Pham, H.-D., Kavak, Y., Pechoušek, J., Machala, L., Zbořil, R., Szenthe, K., Abadía, J., et al., 2019. Chloroplasts preferentially take up ferric – citrate over iron – nicotianamine complexes in *Brassica napus*. Planta 249, 751–763. https://doi.org/10.1007/s00425-018-3037-0.

Pan, I.C., Tsai, H.H., Cheng, Y.T., Wen, T.N., Buckhout, T.J., Schmidt, W., 2015. Post-transcriptional coordination of the *Arabidopsis* iron deficiency response is partially dependent on the E3 ligases RING DOMAIN LIGASE1 (RGLG1) and RING DOMAIN LIGASE2 (RGLG2). Mol. Cell. Proteomics 14, 2733–2752. https://doi.org/10.1074/mcp.M115.048520.

Pavlović, J., Samardzić, J., Maksimović, V., Timotijević, G., Stević, N., Laursen, K.H., Hansen, T.H., Husted, S., Schjoerring, J.K., et al., 2013. Silicon alleviates iron deficiency in cucumber by promoting mobilization of iron in the root apoplast. New Phytol. 198, 1096–1107. https://doi.org/10.1093/aob/mcw105.

Pestana, M., Correia, P.J., Saavedra, T., Gama, F., Abadía, A., de Varennes, A., 2012. Development and recovery of iron deficiency by iron resupply to roots or leaves of strawberry plants. Plant Physiol. Biochem. 53, 1–5. https://doi.org/10.1016/j.plaphy.2012.01.001.

Pfaffl, M.W., 2001. A new mathematical model for relative quantification in real-time RT–PCR. Nucleic Acids Res. 29, e45. https://doi.org/10.1093/nar/29.9.e45.

Rellán-Álvarez, R., Andaluz, S., Rodríguez-Celma, J., Wohlgemuth, G., Zocchi, G., Álvarez-Fernández, A., Fiehn, O., López-Millán, A.F., Abadía, J., 2010. Changes in the proteomic and metabolic profiles of *Beta vulgaris* root tips in response to iron deficiency and resupply. BMC Plant Biol. 10, 1–15. https://doi.org/10.1186/1471-2229-10-120.

Riaz, N., Guerinot, M.L., 2021. All together now: regulation of the iron deficiency response. J. Exp. Bot. 72, 2045–2055. https://doi.org/10.1093/jxb/erab003.

Rodríguez-Celma, J., Lattanzio, G., Grusak, M.A., Abadía, A., Abadía, J., López-Millán, A.F., 2011. Root responses of *Medicago truncatula* plants grown in two different iron deficiency conditions: changes in root protein profile and riboflavin biosynthesis. J. Proteome Res. 10, 2590–2601. https://doi.org/10.1021/pr2000623.

Rodríguez-Celma, J., Lin, W.D., Fu, G.M., Abadía, J., López-Millán, A.F., Schmidt, W., 2013. Mutually exclusive alterations in secondary metabolism are critical for the uptake of insoluble iron compounds by *Arabidopsis* and *Medicago truncatula*. Plant Physiol. 162, 1473–1485. https://doi.org/10.1104/pp.113.220426.

Rodríguez-Celma, J., Chou, H., Kobayashi, T., Long, T.A., Balk, J., 2019. Hemerythrin E3 ubiquitin ligases as negative regulators of iron homeostasis in plants. Front. Plant Sci. 10, 1–7. https://doi.org/10.3389/fpls.2019.00098.

Rui, M., Ma, C., Hao, Y., Guo, J., Rui, Y., Tang, X., Qi, Z., Xing, F., Zhang, Z., et al., 2016. Iron oxide nanoparticles as a potential iron fertilizer for peanut (*Arachis hypogaea*). Front. Plant Sci. 7, 815. https://doi.org/10.3389/fpls.2016.00815.

Santi, S., Schmidt, W., 2009. Dissecting iron deficiency-induced proton extrusion in *Arabidopsis* roots. New Phytol. 183, 1072–1084. https://doi.org/10.1111/j.1469-8137.2009.02908.x.

Satoh, J., Koshino, H., Sekino, K., Ito, S., Katsuta, R., Takeda, K., Yoshimura, E., Shinmachi, F., Kawasaki, S., et al., 2016. *Cucumis sativus* secretes 4′-ketoriboflavin under iron-deficient conditions. Biosci. Biotechnol. Biochem. 80, 363–367. https://doi.org/10.1080/09168451.2015.1095070.

Schagerlöf, U., Wilson, G., Hebert, H., Al-Karadaghi, S., Hägerhäll, C., 2006. Transmembrane topology of FRO2, a ferric chelate reductase from *Arabidopsis thaliana*. Plant Mol. Biol. 62, 215–221. https://doi.org/10.1007/s11103-006-9015-0.

Schwab, F., Zhai, G., Kern, M., Turner, A., Schnoor, J.L., Wiesner, M.R., 2016. Barriers, pathways and processes for uptake, translocation and accumulation of nanomaterials in plants - critical review. Nanotoxicology 10, 257–278. https://doi.org/10.3109/17435390.2015.1048326.

Schwarz, B., Bauer, P., 2020. FIT, a regulatory hub for iron deficiency and stress signaling in roots, and FIT-dependent and -independent gene signatures. J. Exp. Bot. 71, 1694–1705. https://doi.org/10.1093/jxb/eraa012.

Shimizu, K., Tschulik, K., Compton, R.G., 2016. Exploring the mineral–water interface: reduction and reaction kinetics of single hematite (α-Fe_2O_3) nanoparticles. Chem. Sci. 7, 1408–1414. https://doi.org/10.1039/C5SC03678J.

Shinmachi, F., Hasegawa, I., Noguchi, A., Yazaki, J., 1997. Characterization of iron deficiency response system with riboflavin secretion in some dicotyledonous plants. In: Ando, T., Fujita, K., Mae, T., Matsumoto, H., Mori, S., Sekiya, J. (Eds.), Plant Nutrition for Sustainable Food Production and Environment. Springer, Dordrecht, Germany, pp. 277–278. https://doi.org/10.1007/978-94-009-0047-9_79.

Sisó-Terraza, P., Rios, J.J., Abadía, J., Abadía, A., Álvarez-Fernández, A., 2016. Flavins secreted by roots of iron-deficient *Beta vulgaris* enable mining of ferric oxide via reductive mechanisms. New Phytol. 209, 733–745. https://doi.org/10.1111/nph.13633.

Smith, G.F., McCurdy, W.H., Diehl, H., 1952. The colorimetric determination of iron in raw and treated municipal water supplies by use of 4:7-diphenyl-1:10-phenanthroline. Analyst 77, 418–422. https://doi.org/10.1039/AN9527700418.

Solti, Á., Kovács, K., Müller, B., Vázquez, S., Hamar, É., Pham, H.D., Tóth, B., Abadía, J., Fodor, F., 2016. Does a voltage-sensitive outer envelope transport mechanism contributes to the chloroplast iron uptake? Planta 244, 1303–1313. https://doi.org/10.1007/s00425-016-2586-3.

Tombuloglu, H., Anıl, I., Akhtar, S., Turumtay, H., Sabit, H., Slimani, Y., Almessiere, M., Baykal, A., 2020a. Iron oxide nanoparticles translocate in pumpkin and alter the phloem sap metabolites related to oil metabolism. Sci. Hortic. 265, 109223 https://doi.org/10.1016/j.scienta.2020.109223.

Tombuloglu, H., Slimani, Y., AlShammari, T.M., Bargouti, M., Ozdemir, M., Tombuloglu, G., Akhtar, S., Sabit, H., Hakeem, K.R., et al., 2020b. Uptake, translocation, and physiological effects of hematite (α-Fe_2O_3) nanoparticles in barley

(*Hordeum vulgare* L.). Environ. Pollut. 266, 115391 https://doi.org/10.1016/j.envpol.2020.115391.

Vert, G.A., Briat, J.F., Curie, C., 2003. Dual regulation of the *Arabidopsis* high-affinity root iron uptake system by local and long-distance signals. Plant Physiol. 132, 796–804. https://doi.org/10.1104/pp.102.016089.

Vorwieger, A., Gryczka, C., Czihal, A., Douchkov, D., Tiedemann, J., Mock, H.-P., Jakoby, M., Weisshaar, B., et al., 2007. Iron assimilation and transcription factor controlled synthesis of riboflavin in plants. Planta 226, 147–158. https://doi.org/10.1007/s00425-006-0476-9.

Wang, J.W., Grandio, E.G., Newkirk, G.M., Demirer, G.S., Butrus, S., Giraldo, J.P., Landry, M.P., 2019. Nanoparticle-mediated genetic engineering of plants. Mol. Plant 12, 1037–1040. https://doi.org/10.1016/j.molp.2019.06.010.

Waters, B.M., McInturf, S.A., Amundsen, K., 2014. Transcriptomic and physiological characterization of the *fefe* mutant of melon (*Cucumis melo*) reveals new aspects of iron-copper crosstalk. New Phytol. 203, 1128–1145. https://doi.org/10.1111/nph.12911.

Welkie, G.W., 2000. Taxonomic distribution of dicotyledonous species capable of root excretion of riboflavin under iron deficiency. J. Plant Nutr. 23, 1819–1831. https://doi.org/10.1080/01904160009382145.

Xu, G., Jiang, Z., Wang, H., Lin, R., 2019. The central circadian clock proteins CCA1 and LHY regulate iron homeostasis in *Arabidopsis*. J. Integr. Plant Biol. 61, 168–181. https://doi.org/10.1111/jipb.12696.

Yuan, J., Chen, Y., Li, H., Lu, J., Zhao, H., Liu, M., Nechitaylo, G.S., Glushchenko, N.N., 2018. New insights into the cellular responses to iron nanoparticles in *Capsicum annuum*. Sci. Rep. 8, 1–9. https://doi.org/10.1038/s41598-017-18055-w.

Zhu, H., Han, J., Xiao, J.Q., Jin, Y., 2008. Uptake, translocation, and accumulation of manufactured iron oxide nanoparticles by pumpkin plants. J. Environ. Monit. 10, 713–717. https://doi.org/10.1039/B805998E.